J. Fluid Mech. (2024), *vol*. 986, R2, doi:10.1017/jfm.2024.389

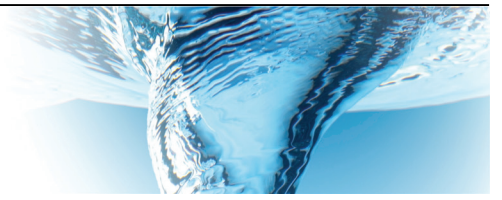

What Rayleigh numbers are achievable under Oberbeck–Boussinesq conditions?

Stephan Weiss[1,2,†], **Mohammad S. Emran**[1] **and Olga Shishkina**[1,†]

[1]Max-Planck Institute for Dynamics and Self-Organization, Am Fassberg 17, 37077 Göttingen, Germany

[2]Institute of Aerodynamics and Flow Technology, German Aerospace Center (DLR), Bunsenstraße 10, 37073 Göttingen, Germany

(Received 7 March 2024; revised 12 April 2024; accepted 15 April 2024)

The validity of the Oberbeck–Boussinesq (OB) approximation in Rayleigh–Bénard (RB) convection is studied using the Gray & Giorgini (*Intl J. Heat Mass Transfer*, vol. 19, 1976, pp. 545–551) criterion that requires that the residuals, i.e. the terms that distinguish the full governing equations from their OB approximations, are kept below a certain small threshold $\hat{\sigma}$. This gives constraints on the temperature and pressure variations of the fluid properties (density, absolute viscosity, specific heat at constant pressure c_p, thermal expansion coefficient and thermal conductivity) and on the magnitudes of the pressure work and viscous dissipation terms in the heat equation, which all can be formulated as bounds regarding the maximum temperature difference in the system, Δ, and the container height, L. Thus for any given fluid and $\hat{\sigma}$, one can calculate the OB-validity region (in terms of Δ and L) and also the maximum achievable Rayleigh number $Ra_{max,\hat{\sigma}}$, and we did so for fluids water, air, helium and pressurized SF_6 at room temperature, and cryogenic helium, for $\hat{\sigma} = 5\,\%$, $10\,\%$ and $20\,\%$. For the most popular fluids in high-Ra RB measurements, which are cryogenic helium and pressurized SF_6, we have identified the most critical residual, which is associated with the temperature dependence of c_p. Our direct numerical simulations (DNS) showed, however, that even when the values of c_p can differ almost twice within the convection cell, this feature alone cannot explain a sudden and strong enhancement in the heat transport in the system, compared with its OB analogue.

Key words: Bénard convection, turbulent convection

† Email addresses for correspondence: Stephan.Weiss@dlr.de, Olga.Shishkina@ds.mpg.de

1. Introduction

Rayleigh–Bénard (RB) convection serves as a quintessential benchmark in fluid physics, spanning instabilities, pattern formation (Bodenschatz, Pesch & Ahlers 2000), transition to turbulence, and fully developed turbulence, including the so-called ultimate regime, which is characterized by extremely intense driving forces in the system, see Ahlers, Grossmann & Lohse (2009*c*), Lohse & Xia (2010), Chillà & Schumacher (2012), Xia (2013), Shishkina (2021) and Lohse & Shishkina (2023). In experiments, RB convection is studied in closed containers, where the top and bottom are kept at constant temperatures, $T = T_+$ at the bottom and $T = T_-$ at the top, $T_- < T_+$, and the sidewalls are thermally isolated. The RB flows are driven by the density differences between the heavier (usually cold) fluid that tends to sink and lighter (usually hot) fluid that tends to rise. The intensity of the thermal driving force is characterized by the Rayleigh number $Ra \equiv \alpha g \Delta L^3/(\nu\kappa)$, a dimensionless measure of the temperature difference in the system, $\Delta \equiv T_+ - T_-$ (here α denotes the thermal expansion coefficient and g acceleration coefficient due to gravity). The other control parameters are the Prandtl number $Pr \equiv \nu/\kappa$ (the ratio of kinematic viscosity ν and thermal diffusivity κ) and the container aspect ratio $\Gamma \equiv D/L$ (the ratio between its width D and height L).

When defining the control parameters Ra and Pr, we already implicitly assume that the fluid properties (e.g. ν, κ and α) do not change throughout the entire volume of the container. However, material properties of any real fluid depend on its temperature and pressure. Within the Oberbeck–Boussinesq (OB) approximation (Oberbeck 1879; Boussinesq 1903), which is usually considered in theories and numerical simulations, the temperature and pressure dependencies of the fluid properties are not taken into account (apart from the density in the buoyancy term of the Navier–Stokes equation, where it is approximated by a linear function of the temperature). This omission might potentially lead to what is known as non-Oberbeck–Boussinesq (NOB) effects, i.e. to noteworthy deviations in heat or momentum transport, or global flow structures, compared with predictions one can draw from the OB equations.

One of the most relevant questions in RB studies is: How do the heat transport (in dimensionless form, the Nusselt number Nu) and momentum transport (the Reynolds number Re) depend on the control parameters Ra, Pr and Γ, especially for extremely large values of Ra, which are relevant in astro- and geophysical flows? The dependencies are usually sought as scaling relations, e.g. $Nu \sim Ra^\gamma$, with γ being the scaling exponent. For Ra up to approximately 10^{11}, the different data sets qualitatively agree and follow predictions of the Grossmann & Lohse (2000, 2001) theory (with prefactors from Stevens *et al.* 2013), but at very large Ra, they show different behaviours. For instance, heat flux measurements using cryogenic helium that were conducted at the University of Oregon (Niemela, Skrbek & Donnelly 2000*a*; Niemela *et al.* 2000*b*,*c*) show no increase in γ for Ra up to 10^{17}. However, very similar measurements with helium conducted in Grenoble (Roche *et al.* 2010; Roche 2020) as well as measurements conducted in sulfphur hexafluoride (SF_6, see Ahlers *et al.* 2009*a*; Ahlers, Funfschilling & Bodenschatz 2009*b*; Ahlers *et al.* 2012*a*,*b*; He *et al.* 2012*a*,*b*; Ahlers, Bodenschatz & He 2014; He *et al.* 2014, 2015; He, Bodenschatz & Ahlers 2016, 2020) show transitions to the ultimate regime with $\gamma \gtrsim 0.4$, although at different Ra. This difference in Ra is recently explained with the non-normal–nonlinear nature of this transition (Roche 2020; Lohse & Shishkina 2023). Another Oregon experiment (Niemela & Sreenivasan 2003) and measurements in Brno (Urban *et al.* 2014, 2019) also showed a significant increase in Nu, with $\gamma > 1/3$; however, the authors tend to explain this phenomenon by NOB effects rather than by the transition to the ultimate regime.

In this article, we will try to provide more clarity on whether the temperature and/or pressure variations of the fluid properties can be decisive in a crucial change in the scaling exponent, from $\gamma \lesssim 1/3$ to $\gamma \gtrsim 0.4$, which is observed in many RB experiments at high $Ra \gtrsim 10^{11}$.

2. Oberbeck–Boussinesq approximation

The OB approximation is a simplified model, incorporating buoyancy effects. It assumes an incompressible flow and introduces two key assumptions. Firstly, it posits that all fluid properties remain constant, except for density in the buoyancy force term of the momentum equation, which is assumed to depend linearly on temperature with the isobaric thermal expansion being the relevant coefficient. Secondly, it disregards the contributions of pressure work and viscous dissipation in the heat equation (see also Roche *et al.* 2010, appendix A2). The OB governing equations for the velocity field $\boldsymbol{u}(\boldsymbol{x}, t)$ (with u_j the velocity components in spatial directions x_j), the temperature field $T(\boldsymbol{x}, t)$ and the hydrodynamic pressure $p(\boldsymbol{x}, t)$ include the following continuity equation, and momentum and heat equations:

$$\boldsymbol{\nabla} \cdot \boldsymbol{u} = 0, \tag{2.1}$$

$$\partial_t \boldsymbol{u} + (\boldsymbol{u} \cdot \boldsymbol{\nabla})\boldsymbol{u} + \boldsymbol{\nabla} p/\rho = \nu \boldsymbol{\nabla}^2 \boldsymbol{u} + \alpha (T - T_0) g \boldsymbol{e}_z, \tag{2.2}$$

$$\partial_t T + (\boldsymbol{u} \cdot \boldsymbol{\nabla}) T = \kappa \boldsymbol{\nabla}^2 T. \tag{2.3}$$

Here ρ is the density, $\nu \equiv \mu/\rho$ the kinematic viscosity, $\kappa \equiv k/(\rho c_p)$ the thermal diffusivity, with μ being the dynamic viscosity, k the thermal conductivity, and c_p the specific heat at constant pressure, and ∂_t denotes the partial derivative in time t, and $\boldsymbol{e}_z$ the unit vector pointing upwards. The reference temperature T_0 is taken at the arithmetic mean of the top and bottom temperatures, $T_0 \equiv (T_+ + T_-)/2$.

Starting from the works of Spiegel & Veronis (1960) and Veronis (1962), the validity of the OB approximation (2.1)–(2.3) has been scrutinized in various theoretical studies, where the magnitudes of specific terms in the governing equations were examined. A rigorous mathematical variational approach, employing expansions of fluid properties as power series, was initially introduced by Mihaljan (1962), who primarily focused on the temperature dependency of the density. Subsequently, other researchers extended the method to incorporate pressure and temperature dependencies of other fluid parameters.

When moving beyond the OB approximation, a simple exploration involves considering a first-order linear dependence on both temperature and pressure, of each material property φ,

$$\frac{\varphi}{\varphi_0} = 1 + \varepsilon_{\varphi,T} \frac{T - T_0}{\Delta} + \varepsilon_{\varphi,P} \frac{P - P_0}{\rho_0 g L}, \tag{2.4}$$

including the density ($\varphi = \rho$), absolute viscosity ($\varphi = \mu$), specific heat at constant pressure ($\varphi = c_p$), thermal expansion coefficient ($\varphi = \alpha$), and thermal conductivity ($\varphi = k$), and $\kappa \equiv k/(\rho c_p)$ is a dependent parameter, fully determined by k, ρ and c_p (Gray & Giorgini 1976). Thus the manifestation of non-Oberbeck–Boussinesqness (NOBness) is determined by different dimensionless factors $\varepsilon_{\varphi,T}$ and $\varepsilon_{\varphi,p}$. When dealing with a specific fluid under given operational conditions of reference temperature T_0 and pressure P_0, it is not immediately evident which among these parameters $\varepsilon_{\varphi,T}$ and $\varepsilon_{\varphi,p}$ is most relevant in inducing NOBness in the experimental set-up. (The fluid properties at the reference T_0 and P_0 will be denoted in the following with a subscript '0'.) Unravelling the diverse NOB effects is possible in direct numerical simulations (DNS) which allow for the use of

artificial fluids that exhibit only a single specific source of NOBness. For instance, Ahlers *et al.* (2008) conducted such an investigation for ethane. Various studies have explored NOB effects in RB convection in cryogenic helium and pressurized SF_6 (Roche *et al.* 2010; Shishkina, Weiss & Bodenschatz 2016; Weiss *et al.* 2018; Roche 2020; Yik, Valori & Weiss 2020), as well as in water and glycerol (Manga & Weeraratne 1999; Ahlers *et al.* 2006; Sugiyama *et al.* 2009; Horn, Shishkina & Wagner 2013; Horn & Shishkina 2014).

In experiments, the NOB effects are always present (although they can be negligible) and currently, there is no established method for precisely estimating their influence in heat transport measurements. However, it is possible to estimate *a priori* the values of $\varepsilon_{\varphi,T}$ and $\varepsilon_{\varphi,p}$ and set thresholds for their maximal values in an experiment. Note that in some studies only the temperature variation of the density ($\alpha\Delta$) is considered as a measure of NOBness (e.g. Niemela & Sreenivasan 2003); however, it is only one ($\varepsilon_{\rho,T}$) of in total ten sources of NOBness (all parameters $\varepsilon_{\varphi,T}$ and $\varepsilon_{\varphi,P}$).

To study the validity of the OB approximation, we follow a comprehensive variational approach suggested by Gray & Giorgini (1976). We start with the governing equations for a flow of a Newtonian fluid of variable properties (§ 15, Chapter II of Landau & Lifshitz 1987):

$$D_t\rho + \rho\nabla\cdot\boldsymbol{u} = 0, \tag{2.5}$$

$$\rho D_t\boldsymbol{u} + \nabla P = \nabla\cdot(\mu\boldsymbol{S}) - \rho g\boldsymbol{e}_z + \nabla(\eta\,\nabla\cdot\boldsymbol{u}), \tag{2.6}$$

$$\rho c_p D_t T = \nabla\cdot(k\nabla T) + \alpha T D_t P + \mu\Phi, \tag{2.7}$$

where $P = p - \rho_0 g z\boldsymbol{e}_z$ is the (full) pressure, $\boldsymbol{S}$ the deformation rate tensor with components, $S_{ij} \equiv \partial_j u_i + \partial_i u_j - (2\delta_{ij}/3)\partial_k u_k$, $\Phi \equiv (S_{ij}/2)(\partial_j u_i + \partial_i u_j)$ the viscous dissipation function, $D_t \equiv \partial_t + \boldsymbol{u}\cdot\nabla$ denotes the full (material) derivative, δ_{ij} the Kronecker symbol, and η the second viscosity. As it has been shown by Spiegel & Veronis (1960), the last term in (2.6) can be neglected if pressure fluctuations are smaller then static variation, which is the case for relatively slow convective flows. Therefore, we assume that the last term in (2.6), which is associated with the second viscosity η, vanishes.

Substituting the linear representations (2.4) of the fluid properties $\varphi = \rho$, μ, c_p, α and k into (2.5)–(2.7), one requires that the residuals, i.e. the terms that distinguish the resulting equations from their OB approximation (2.1)–(2.3), are negligibly small. The OB requirements are fulfilled if not only all $\varepsilon_{\varphi,T}$ and $\varepsilon_{\varphi,P}$ are negligibly small, but also the magnitudes of the pressure work term ($\alpha T\,D_t P$) and of the dissipation term ($\mu\Phi$) in (2.7) are negligibly small compared with the magnitudes of the other terms in (2.7). Comparing $\rho c_p D_t T$ with $\alpha T\,D_t P$ in (2.7), we conclude that the pressure work is negligible if $\rho_0 c_{p,0}\Delta \gg \alpha_0 T_0 \rho_0 g L$ (here we estimate the pressure magnitude as $P \sim \rho_0 g L$ and the magnitudes of the temperature variation as Δ and of the absolute value of the temperature as T_0). Comparing $\nabla\cdot(k\,\nabla T)$ with $\mu\Phi$, we conclude that the dissipation term is negligible if $k_0\Delta \gg \mu_0\alpha_0 g\Delta L$ (here the velocity magnitude is estimated as the free-fall velocity $\sqrt{\alpha_0 g L\Delta}$). The last two inequalities can be reformulated, respectively, as $bT_0/\Delta \ll 1$ and $bPr_0 \ll 1$, where $Pr_0 \equiv \nu_0/\kappa_0$ is the reference Prandtl number, $\kappa_0 \equiv k_0/(\rho_0\,c_{p,0})$ is the reference thermal diffusivity and $b \equiv \alpha_0 g L/c_{p,0}$.

Introducing a certain small threshold on the degree of NOBness $\hat{\sigma}$, $0 < \hat{\sigma} \ll 1$, we say that the OB approximation is valid with the accuracy $\hat{\sigma}$, if requirements (2.8)–(2.9) are fulfilled:

$$\varepsilon_{\varphi,T} < \hat{\sigma}, \quad \varepsilon_{\varphi,P} < \hat{\sigma}, \quad \text{for } \varphi = \rho, \mu, c_p, k, \tag{2.8}$$

$$bT_0/\Delta < \hat{\sigma}, \quad bPr_0 < \hat{\sigma}. \tag{2.9}$$

Relations (2.8)–(2.9) are derived by substituting (2.4) for all fluid properties φ into (2.5)–(2.7) and requiring that the terms, which are not present in the OB approximation (2.1)–(2.3), become negligibly small when the measure of the NOBness $\hat{\sigma}$ becomes infinitesimal, $\hat{\sigma} \to 0$.

3. The validity of the Oberbeck–Boussinesq approximation for different set-ups

For any given fluid and threshold $\hat{\sigma}$ for the residuals, from (2.8)–(2.9) one can derive the OB-validity region in terms of the maximally possible temperature difference Δ in the system and height L of the container. Here, to capture the NOB effects, we confine our examination to the lowest order, (2.4), focusing solely on a linear term in the temperature and pressure expansions of the fluid properties. This is sufficient, as shown in a recent study by Macek *et al.* (2023) for the case of cryogenic helium.

In figure 1 the OB-regions are calculated for operational conditions typically employed in RB experiments and some fluids, namely, for water, air, ethane, helium, pressurized gas sulphur hexafluoride (SF_6) at room temperatures, and cryogenic helium, using REFPROP (2013). For any given fluid and reference temperature T_0 and pressure P_0, the OB-validity regions depend on the OB threshold $\hat{\sigma}$. The choices $\hat{\sigma} = 5\,\%$, $\hat{\sigma} = 10\,\%$ and $\hat{\sigma} = 20\,\%$ give the embedded OB-validity domains coloured, respectively, green, blue and red in figure 1 (see also sketch in figure 4(*a*) in Ecke & Shishkina 2023). There, each triangularly shaped OB-validity domain is bounded from the right and left by maximum admissible variations of the fluid properties with the temperature (vertical line) and by maximum admissible pressure work term in the heat equation (inclined line), respectively. The lower boundary is determined by the onset of convection, which is calculated in figure 1 for an infinite horizontally extended fluid layer, such that $Ra_c \approx 1708$. For any laterally bounded domain, this boundary moves up, since the critical Ra_c for the onset of convection scales as $\sim \Gamma^{-4}$ for $\Gamma \to 0$ (Shishkina 2021; Ahlers *et al.* 2022).

The boundedness of the OB-validity region restricts the maximal Ra, which can be reached in almost-OB experiments. This means that for any chosen fluid and threshold on the degree of NOBness (parameter $\hat{\sigma}$), Rayleigh numbers Ra larger than a certain maximum value $Ra_{max,\,\hat{\sigma}}$ can in principle not be realized experimentally. In figure 1, these $Ra_{max,\hat{\sigma}}$ values are achieved in the upper corners of each OB-validity region, and each value of $Ra_{max,\hat{\sigma}}$ is written in the plots with the colour of the corresponding OB-validity region.

By comparing the values of $Ra_{max,\hat{\sigma}}$ among the analysed fluids in figure 1, it can be inferred that water emerges as the optimal fluid for investigating RB convection under OB conditions at extreme Ra, owing to its highest $Ra_{max,\hat{\sigma}}$. Nonetheless, we note that achieving such exceedingly high Ra is feasible only when the water layer's depth is several hundred metres. Considering this limitation, the utilization of cryogenic helium and pressurized SF_6 becomes more advantageous for experimental inquiries into the transition to the ultimate regime. In figure 2, by examples of pressurized SF_6 (used in Göttingen experiments) and cryogenic helium (used in other studies of the ultimate regime, including Oregon, Grenoble and Brno) we show the dependencies of $Ra_{max,\hat{\sigma}}$ on the reference temperature T_0 and pressure P_0. One sees, in particular, that keeping the operating pressure P_0 in a range between 10 bar and 15 bar in experiments with SF_6 is favourable in the sense that this allows higher values of Ra under (almost) OB conditions to be achieved. In all studied cases, we found that pressure variations of the fluid properties are negligible compared with their temperature variations.

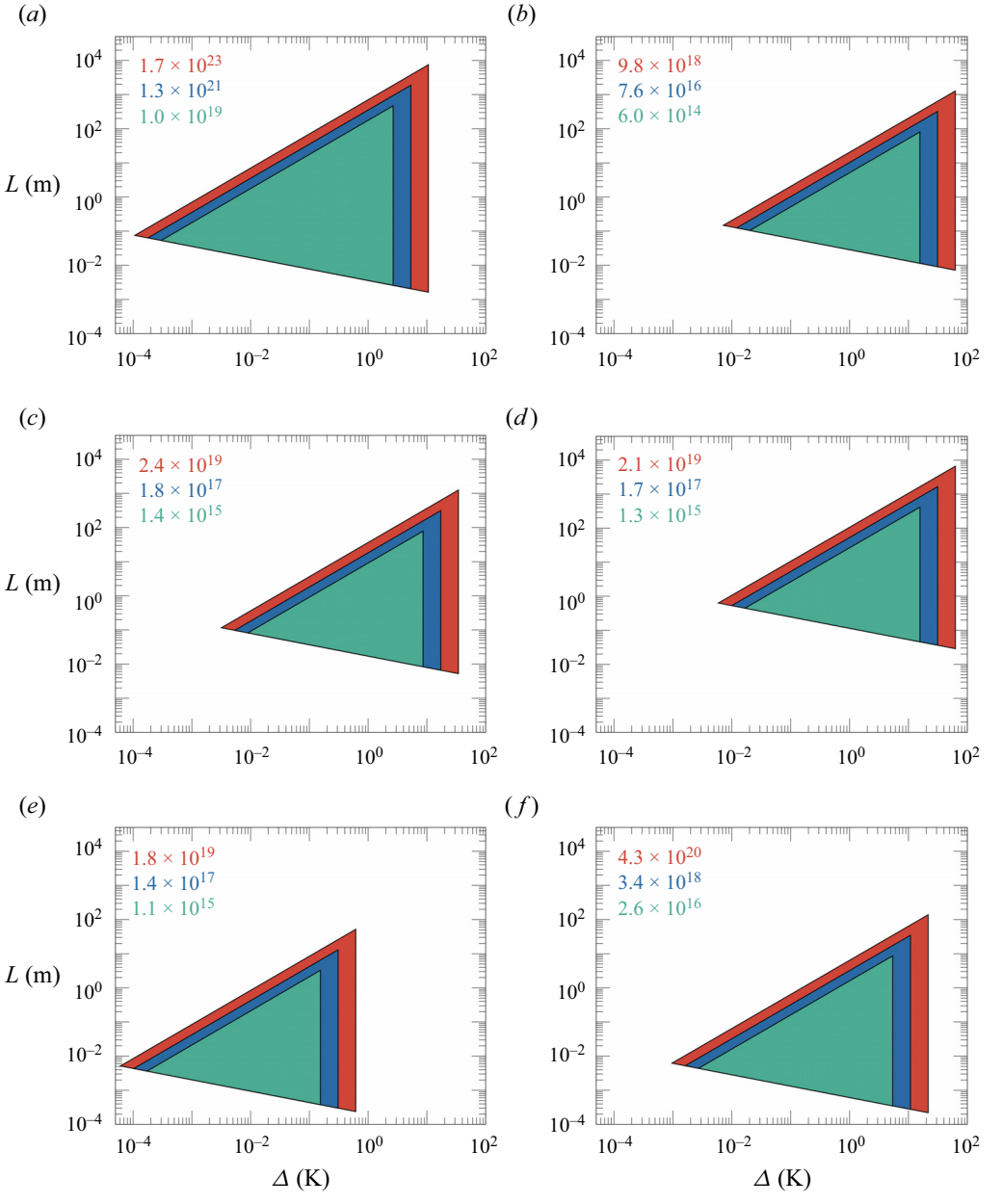

Figure 1. Regions of the validity of the OB approximation, in terms of the maximum temperature difference, Δ, and container height, L, according to (2.8)–(2.9), for different fluids: (*a*) water at $T_0 = 40\,^\circ$C and $P_0 = 1$ bar, (*b*) air at $T_0 = 40\,^\circ$C and $P_0 = 1$ bar, (*c*) ethane at $T_0 = 40\,^\circ$C and $P_0 = 1$ bar, (*d*) helium at $T_0 = 40\,^\circ$C and $P_0 = 1$ bar, (*e*) helium at $T_0 = -268.15\,^\circ\text{C} = 5$ K and $P_0 = 1$ bar, (*f*) SF_6 at $T_0 = 30\,^\circ$C and $P_0 = 20$ bar. The nested green, blue and red OB-validity regions correspond, respectively, to the thresholds on the degree of NOBness $\hat{\sigma} = 5\,\%$, $10\,\%$ and $20\,\%$. The lower boundaries of these regions have the slopes $L \propto \Delta^{-1/3}$, the left boundaries $L \propto \Delta$, and the right ones are vertical. The values of the maximum achievable Rayleigh numbers, $Ra_{max,\hat{\sigma}}$, are written with the corresponding colours.

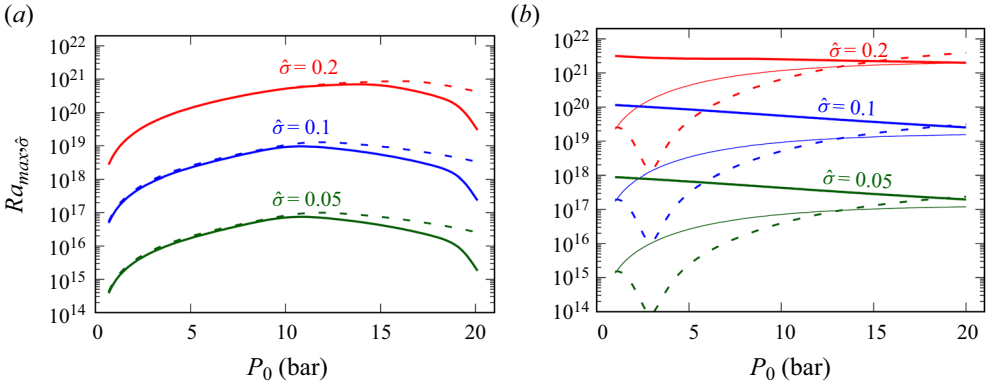

Figure 2. Maximum achievable Rayleigh numbers $Ra_{max,\hat{\sigma}}$, as functions of the reference pressure P_0, for different thresholds on the degree of NOBness: $\hat{\sigma} = 5\,\%$ (green), $\hat{\sigma} = 10\,\%$ (blue) and $\hat{\sigma} = 20\,\%$ (red), for (*a*) gaseous SF_6 (solid lines for $T_0 = 20\,^\circ$C and dashed lines for $T_0 = 30\,^\circ$C) and (*b*) cryogenic helium (thick lines for $T_0 = 2.5$ K, thin lines for $T_0 = 4.0$ K and dashed lines for $T_0 = 5.5$ K). The continuous lines show the liquid phase only, while the dashed lines correspond to both phases, gas and liquid, showing a V-shape near the critical pressure $P_c \approx 2.27$ bar, where the fluid properties become very sensitive to the temperature and pressure variations.

4. The effect of the temperature dependency of c_p on the measured Nu

Among all fluid properties, the specific heat capacity c_p was found to have the strongest variations with the temperature (i.e. $\varepsilon_{c_p,T}$ is significantly larger than any other $\varepsilon_{\varphi,T}$ or $\varepsilon_{\varphi,P}$), for both considered fluids, which are pressurized SF_6 and cryogenic helium.

For each of the two considered fluids, we selected two cases (characterized by P_0 and $[T_-, T_+]$) that correspond to some representative Göttingen or Brno measurements: one case is the 'classical' one, where the heat transport scaling exponent $\gamma < 1/3$ was measured, and the other case we call 'ultimate', where $\gamma \gtrsim 0.4$ was measured, see figure 3. In the classical cases, $c_p(T)$ is almost flat, while in the ultimate cases it rapidly decreases with increasing temperature, for both, SF_6 and helium. By example of these four cases (classical and ultimate, for both, pressurized SF_6 and cryogenic helium) we want to investigate in DNS whether the strong temperature variation of c_p alone (as in the ultimate cases) can significantly increase the heat transport and with this alter the scaling exponent γ in the $Nu \sim Ra^\gamma$ relation.

Assuming that for any small $\hat{\sigma} > 0$, all requirements (2.8)–(2.9) are fulfilled apart from the variation of c_p with the temperature, so that $\varphi_{c_p,T}$ is not negligible, we obtain the governing equations, which are similar to the OB equations (2.1)–(2.3), but with

$$(c_p(T)/c_{p,0})[\partial_t T + (\boldsymbol{u}\cdot\boldsymbol{\nabla})T] = \kappa_0 \boldsymbol{\nabla}^2 T \tag{4.1}$$

instead of (2.3). (In terms of independent fluid parameters, (4.1) can be rewritten as $c_p(T)[\partial_t T + (\boldsymbol{u}\cdot\boldsymbol{\nabla})T] = (k_0/\rho_0)\boldsymbol{\nabla}^2 T$.)

The four profiles of $c_p(T)/c_{p,0}$ (classical and ultimate, for pressurized SF_6 and cryogenic helium, cf. figure 3*b*,*d*) are approximated by polynomials

$$\frac{c_p(T)}{c_{p,0}} = 1 + \sum_{j=1}^{3} c_j \left(\frac{T - T_0}{\Delta}\right)^j, \tag{4.2}$$

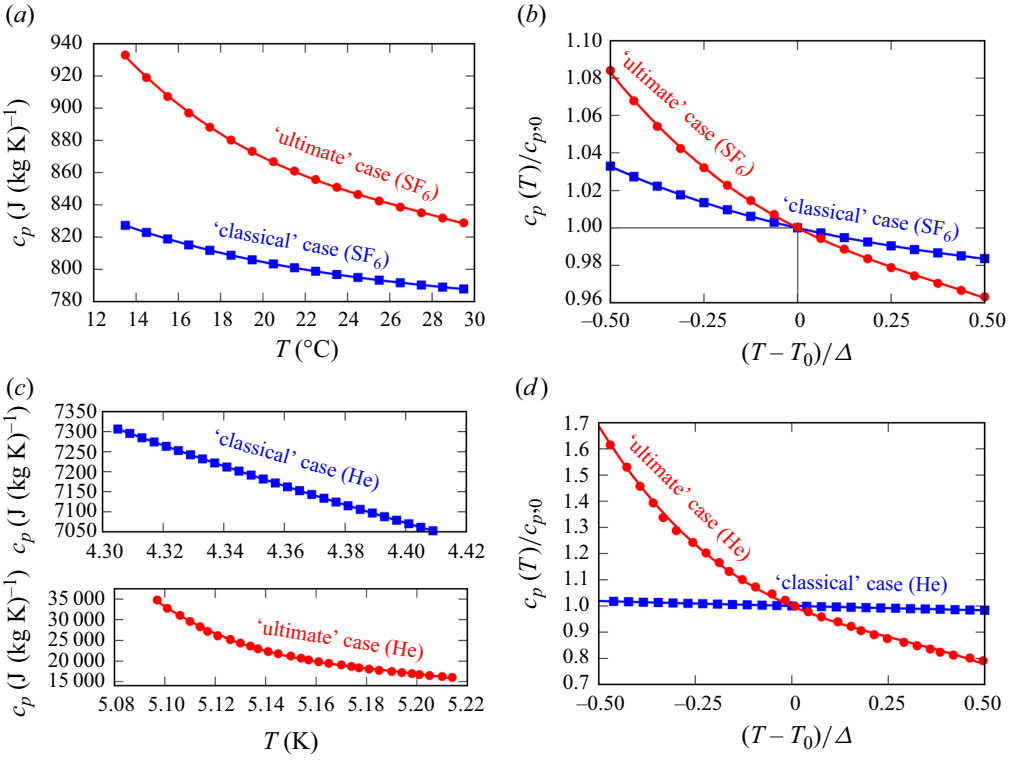

Figure 3. (*a*,*c*) Specific heat capacity c_p as functions of the temperature T, in the classical case (blue symbols) and ultimate case (red symbols), for (*a*) SF_6 for $T \in [13.49\,^\circ\mathrm{C}, 29.49\,^\circ\mathrm{C}]$ and pressure $P_0 = 15.28$ bar (classical) and $P_0 = 17.68$ bar (ultimate), and for (*c*) cryogenic helium for $T \in [4.305\,\mathrm{K},\ 4.409\,\mathrm{K}]$ and $P_0 = 0.8137$ bar (classical), and $T \in [5.097\,\mathrm{K},\ 5.214\,\mathrm{K}]$ and $P_0 = 2.0724$ bar (ultimate). (*b*,*d*) Non-dimensionalized data from (*a*,*c*), respectively.

with c_j being the respective coefficients. This together with (2.1)–(2.2) and (4.1) leads to the Nusselt number

$$Nu = \frac{L}{\kappa_0 \Delta}\left\langle u_z(T - T_0)\left(1 + \sum_{j=1}^{3} \frac{c_j}{j+1}\left(\frac{T - T_0}{\Delta}\right)^j\right) - \kappa_0 \frac{\partial T}{\partial z}\right\rangle_{S_z,t}, \tag{4.3}$$

where u_z is a component of the velocity field in the vertical direction z, and $\langle \cdots \rangle_{S_z,t}$ means the averaging in time and over any horizontal cross-section S_z.

We conducted DNS of RB convection in a cubic domain, for $Ra = 10^6$, 10^7, 10^8, 10^9 and 10^{10}, and Prandtl number $Pr = 1$, according to (2.1)–(2.2) and (4.1) and for the four temperature profiles of $c_p(T)/c_p(T_0)$ as in figure 3(*b*,*d*), to check whether the ultimate profiles of $c_p(T)$ can significantly increase the Nusselt numbers compared with the classical profiles. For this purpose, we used the computational code GOLDFISH (Shishkina *et al.* 2015; Reiter & Shishkina 2020; Reiter, Zhang & Shishkina 2022) with sufficiently fine computational grids (Shishkina *et al.* 2010; Kooij *et al.* 2018) that have at least 14 grid points in each boundary layer and 128^3, 192^3, 256^3, 360^3 and 576^3 grid points in total for $Ra = 10^6$, 10^7, 10^8, 10^9 and 10^{10}, respectively.

We expected that the classical profiles of $c_p(T)$ would lead to results close to those from the OB approximation, but the ultimate profiles would lead to visible NOB effects,

Ra	Nu_{OB}	$Nu_{SF_6}^{\text{'ultimate'}}$	$Nu_{SF_6}^{\text{'classical'}}$	$Nu_{Helium}^{\text{'ultimate'}}$	$Nu_{Helium}^{\text{'classical'}}$	d_{SF_6}	d_{Helium}
10^6	8.100 ± 0.003	8.20 ± 0.006	8.22 ± 0.002	8.39 ± 0.006	8.27 ± 0.003	1.2 %	3.6 %
10^7	16.37 ± 0.002	16.40 ± 0.004	16.40 ± 0.008	16.65 ± 0.02	16.46 ± 0.01	0.2 %	1.7 %
10^8	31.65 ± 0.017	31.63 ± 0.02	31.66 ± 0.005	31.97 ± 0.01	31.58 ± 0.006	−0.1 %	1.0 %
10^9	62.44 ± 0.003	62.24 ± 0.04	62.22 ± 0.074	62.92 ± 0.23	62.27 ± 0.09	−0.3 %	0.8 %
10^{10}	127.63 ± 0.05	127.42 ± 0.07	—	128.38 ± 0.29	—	−0.2 %	0.6 %

Table 1. Nusselt numbers Nu obtained for different Ra and fluids (pressurized SF_6 and cryogenic helium), and the classical or ultimate profiles of c_p, see the main text. Statistics is collected over a duration of at least 800 free-fall time units and at least 5 samples per time unit. The relative difference d is defined as $d \equiv (Nu^{\text{'ultimate'}} - Nu_{OB})/Nu_{OB}$. The error σ (standard deviation of $Nu(z)$ profile) is calculated as $\sigma^2 = (1/(N_z - 1))\sum_{n=1}^{N_z}(Nu - \langle Nu\rangle_{S_z,t})^2$, where N_z is the total number of grid points in the vertical direction z.

in particular, to clear differences in the heat transport. Surprisingly enough we failed to recognise any NOB effects or any tendency associated with the NOBness that increases with growing Ra; we found it neither for the classical profiles, nor for the ultimate ones, see table 1. Of course, different DNS show slightly different values of Nu, but there is no pattern that indicates the growth of the scaling exponent γ for the ultimate profiles compared with the classical ones.

5. Conclusions

To sum up, for any fluid and any reasonable threshold for NOBness $\hat{\sigma}$, the OB-validity region is a bounded domain in the parameter plane of the maximum temperature difference in the system, Δ, and the container height, L. This also bounds the maximum achievable Rayleigh number $Ra_{max,\hat{\sigma}}$. We calculated $Ra_{max,\hat{\sigma}}$ for water, air, helium and pressurized SF_6 at room temperature, and cryogenic helium, for $\hat{\sigma} = 5\,\%$, $10\,\%$ and $20\,\%$.

For pressurized SF_6 and cryogenic helium, we found that the pressure variation of the fluid properties is negligible. With respect to the temperature variations, the specific heat, c_p, is the most sensitive for these fluids. Our DNS, however, showed that the strong temperature variation of c_p does not alter the heat transport. Our DNS results therefore do not support the proposition that solely the NOB effects are responsible for the huge growth of Nu (with a significant growth of the scaling exponent γ in the $Nu \sim Ra^{\gamma}$ relation) which was measured in the Göttingen and Brno experiments at the largest Ra values. This growth can be explained by the transition to the ultimate regime and the difference in Ra, at which this transition happens in different experiments, can be explained by the non-normal–nonlinear nature of this transition rather than purely by the NOB effects (Roche 2020; Lohse & Shishkina 2023).

Supplementary material. Supplementary material is available at https://doi.org/10.1017/jfm.2024.389.

Acknowledgements. We thank E. Bodenschatz and D. Lohse for fruitful discussions and D. van Gils for an improvement of figure 1.

Funding. We gratefully acknowledge financial support from the German Research Foundation (DFG) under the grants Sh405/16 and Sh405/22, and the use of computing clusters at The Max Planck Computing and Data Facility (MPCDF) in Munich.

Declaration of interests. The authors report no conflict of interest.

Author ORCIDs.
Stephan Weiss https://orcid.org/0000-0003-1626-3780;
Olga Shishkina https://orcid.org/0000-0002-6773-6464.

References

Ahlers, G., *et al.* 2022 Aspect ratio dependence of heat transfer in a cylindrical Rayleigh–Bénard cell. *Phys. Rev. Lett.* **128**, 084501.

Ahlers, G., Bodenschatz, E., Funfschilling, D., Grossmann, S., He, X., Lohse, D., Stevens, R.J.A.M. & Verzicco, R. 2012*a* Logarithmic temperature profiles in turbulent Rayleigh–Bénard convection. *Phys. Rev. Lett.* **109**, 114501.

Ahlers, G., Bodenschatz, E., Funfschilling, D. & Hogg, J. 2009*a* Turbulent Rayleigh–Bénard convection for a Prandtl number of 0.67. *J. Fluid Mech.* **641**, 157–167.

Ahlers, G., Bodenschatz, E. & He, X. 2014 Logarithmic temperature profiles of turbulent Rayleigh–Bénard convection in the classical and ultimate state for a Prandtl number of 0.8. *J. Fluid Mech.* **758**, 436–467.

Ahlers, G., Brown, E., Araujo, F.F., Funfschilling, D., Grossmann, S. & Lohse, D. 2006 Non-Oberbeck–Boussinesq effects in strongly turbulent Rayleigh–Bénard convection. *J. Fluid Mech.* **569**, 409–446.

Ahlers, G., Calzavarini, E., Araujo, F.F., Funfschilling, D., Grossmann, S., Lohse, D. & Sugiyama, K. 2008 Non-Oberbeck–Boussinesq effects in turbulent thermal convection in ethane close to the critical point. *Phys. Rev.* E **77**, 046302.

Ahlers, G., Funfschilling, D. & Bodenschatz, E. 2009*b* Transitions in heat transport by turbulent convection at Rayleigh numbers up to 10^{15}. *New J. Phys.* **11**, 123001.

Ahlers, G., Grossmann, S. & Lohse, D. 2009*c* Heat transfer and large scale dynamics in turbulent Rayleigh–Bénard convection. *Rev. Mod. Phys.* **81**, 503–537.

Ahlers, G., He, X., Funfschilling, D. & Bodenschatz, E. 2012*b* Heat transport by turbulent Rayleigh–Bénard convection for $Pr \sim 0.8$ and $3 \times 10^{12} \lesssim Ra \lesssim 10^{15}$: aspect ratio $\Gamma = 0.50$. *New J. Phys.* **14**, 103012.

Bodenschatz, E., Pesch, W. & Ahlers, G. 2000 Recent developments in Rayleigh–Bénard convection. *Annu. Rev. Fluid Mech.* **32**, 709–778.

Boussinesq, J. 1903 *Théorie analytique de la chaleur*. Gauthier-Villars.

Chillà, F. & Schumacher, J. 2012 New perspectives in turbulent Rayleigh–Bénard convection. *Eur. Phys. J.* E **35**, 58.

Ecke, R.E. & Shishkina, O. 2023 Turbulent rotating Rayleigh–Bénard convection. *Annu. Rev. Fluid Mech.* **55**, 603–638.

Gray, D.D. & Giorgini, A. 1976 The validity of the Boussinesq approximation for liquids and gases. *Intl J. Heat Mass Transfer* **19**, 545–551.

Grossmann, S. & Lohse, D. 2000 Scaling in thermal convection: a unifying theory. *J. Fluid Mech.* **407**, 27–56.

Grossmann, S. & Lohse, D. 2001 Thermal convection for large Prandtl numbers. *Phys. Rev. Lett.* **86**, 3316–3319.

He, X., Bodenschatz, E. & Ahlers, G. 2016 Azimuthal diffusion of the large-scale-circulation plane, and absence of significant non-Boussinesq effects, in turbulent convection near the ultimate-state transition. *J. Fluid Mech.* **791**, R3.

He, X., Bodenschatz, E. & Ahlers, G. 2020 Aspect ratio dependence of the ultimate-state transition in turbulent thermal convection. *Proc. Natl Acad. Sci. USA* **117**, 30022.

He, X., Funfschilling, D., Bodenschatz, E. & Ahlers, G. 2012*a* Heat transport by turbulent Rayleigh–Bénard convection for $Pr \sim 0.8$ and $4 \times 10^{11} \lesssim Ra \lesssim 2 \times 10^{14}$: ultimate-state transition for aspect ratio $\Gamma = 1.00$. *New J. Phys.* **14**, 063030.

He, X., Funfschilling, D., Nobach, H., Bodenschatz, E. & Ahlers, G. 2012*b* Transition to the ultimate state of turbulent Rayleigh–Bénard convection. *Phys. Rev. Lett.* **108**, 024502.

He, X., van Gils, D.P.M., Bodenschatz, E. & Ahlers, G. 2014 Logarithmic spatial variations and universal f^{-1} power spectra of temperature fluctuations in turbulent Rayleigh–Bénard convection. *Phys. Rev. Lett.* **112**, 174501.

He, X., van Gils, D.P.M., Bodenschatz, E. & Ahlers, G. 2015 Reynolds numbers and the elliptic approximation near the ultimate state of turbulent Rayleigh–Bénard convection. *New J. Phys.* **17** (6), 063028.

HORN, S. & SHISHKINA, O. 2014 Rotating non-Oberbeck–Boussinesq Rayleigh–Bénard convection in water. *Phys. Fluids* **26**, 055111.

HORN, S., SHISHKINA, O. & WAGNER, C. 2013 On non-Oberbeck–Boussinesq effects in three-dimensional Rayleigh–Bénard convection in glycerol. *J. Fluid Mech.* **724**, 175–202.

KOOIJ, G.L., BOTCHEV, M.A., FREDERIX, E.M.A., GEURTS, B.J., HORN, S., LOHSE, D., VAN DER POEL, E.P., SHISHKINA, O., STEVENS, R.J.A.M. & VERZICCO, R. 2018 Comparison of computational codes for direct numerical simulations of turbulent Rayleigh–Bénard convection. *Comput. Fluids* **166**, 1–8.

LANDAU, L.D. & LIFSHITZ, E.M. 1987 *Fluid Mechanics*, 2nd edn., Course of Theoretical Physics, vol. 6. Butterworth Heinemann.

LOHSE, D. & SHISHKINA, O. 2023 Ultimate turbulent thermal convection. *Phys. Today* **76** (11), 26–32.

LOHSE, D. & XIA, K.-Q. 2010 Small-scale properties of turbulent Rayleigh–Bénard convection. *Annu. Rev. Fluid Mech.* **42**, 335–364.

MACEK, M., ZINCHENKO, G., MUSILOVA, V., URBAN, P. & SCHUMACHER, J. 2023 Assessing non-Oberbeck–Boussinesq effects of convection in cryogenic helium. *Phys. Rev. Fluids* **8**, 094606.

MANGA, M. & WEERARATNE, D. 1999 Experimental study of non-Boussinesq Rayleigh–Bénard convection at high Rayleigh and Prandtl numbers. *Phys. Fluids* **11** (10), 2969–2976.

MIHALJAN, J.M. 1962 A rigorous exposition of the Boussinesq approximations applicable to a thin layer of fluid. *Astrophys. J.* **136**, 1126–1133.

NIEMELA, J.J., SKRBEK, L. & DONNELLY, R.J. 2000*a* Ultra-high Rayleigh number convection in cryogenic helium gas. *Physica* B **284–288**, 61–62.

NIEMELA, J.J., SKRBEK, L., SREENIVASAN, K.R. & DONNELLY, R.J. 2000*b* Turbulent convection at very high Rayleigh numbers. *Nature* **404**, 837–841.

NIEMELA, J.J., SKRBEK, L., SWANSON, C., HALL, S., SREENIVASAN, K.R. & DONNELLY, R.J. 2000*c* New results in cryogenic helium flows at ultra-high Reynolds and Rayleigh numbers. *J. Low Temp. Phys.* **121**, 417–422.

NIEMELA, J.J. & SREENIVASAN, K.R. 2003 Confined turbulent convection. *J. Fluid Mech.* **481**, 355–384.

OBERBECK, A. 1879 Über die Wärmeleitung der Flüssigkeiten bei Berücksichtigung der Strömungen in Folge von Temperaturdifferenzen. *Ann. Phys. (Berlin)* **243** (6), 271–292.

REFPROP 2013 NIST Reference fluid thermodynamic and transport properties database. National Institute of Standards and Technology, version 9.1.

REITER, P. & SHISHKINA, O. 2020 Classical and symmetrical horizontal convection: detaching plumes and oscillations. *J. Fluid Mech.* **892**, R1.

REITER, P., ZHANG, X. & SHISHKINA, O. 2022 Flow states and heat transport in Rayleigh–Bénard convection with different sidewall boundary conditions. *J. Fluid Mech.* **936**, A32.

ROCHE, P.-E. 2020 The ultimate state of convection: a unifying picture of very high Rayleigh numbers experiments. *New J. Phys.* **22** (7), 073056.

ROCHE, P.-E., GAUTHIER, F., KAISER, R. & SALORT, J. 2010 On the triggering of the ultimate regime of convection. *New J. Phys.* **12** (8), 085014.

SHISHKINA, O. 2021 Rayleigh–Bénard convection: the container shape matters. *Phys. Rev. Fluids* **6**, 090502.

SHISHKINA, O., HORN, S., WAGNER, S. & CHING, E.S.C. 2015 Thermal boundary layer equation for turbulent Rayleigh–Bénard convection. *Phys. Rev. Lett.* **114**, 114302.

SHISHKINA, O., STEVENS, R.J.A.M., GROSSMANN, S. & LOHSE, D. 2010 Boundary layer structure in turbulent thermal convection and its consequences for the required numerical resolution. *New J. Phys.* **12**, 075022.

SHISHKINA, O., WEISS, S. & BODENSCHATZ, E. 2016 Conductive heat flux in measurements of the Nusselt number in turbulent Rayleigh–Bénard convection. *Phys. Rev. Fluids* **1**, 062301(R).

SPIEGEL, E.A. & VERONIS, G. 1960 On the Boussinesq approximation for a compressible fluid. *Astrophys. J.* **131**, 442–447.

STEVENS, R.J.A.M., VAN DER POEL, E.P., GROSSMANN, S. & LOHSE, D. 2013 The unifying theory of scaling in thermal convection: the updated prefactors. *J. Fluid Mech.* **730**, 295–308.

SUGIYAMA, K., CALZAVARINI, E., GROSSMANN, S. & LOHSE, D. 2009 Flow organization in two-dimensional non-Oberbeck–Boussinesq Rayleigh–Bénard convection in water. *J. Fluid Mech.* **637**, 105–135.

URBAN, P., HANZELKA, P., KRÁLÍK, T., MACEK, M., MUSILOVÁ, V. & SKRBEK, L. 2019 Elusive transition to the ultimate regime of turbulent Rayleigh–Bénard convection. *Phys. Rev.* E **99** (1), 011101.

URBAN, P., HANZELKA, P., MUSILOVÁ, V., KRÁLÍK, T., MANTIA, M.L., SRNKA, A. & SKRBEK, L. 2014 Heat transfer in cryogenic helium gas by turbulent Rayleigh–Bénard convection in a cylindrical cell of aspect ratio 1. *New J. Phys.* **16**, 053042.

VERONIS, G. 1962 The magnitude of the dissipation terms in the Boussinesq approximation. *Astrophys J.* **135**, 655–656.

WEISS, S., HE, X., AHLERS, G., BODENSCHATZ, E. & SHISHKINA, O. 2018 Bulk temperature and heat transport in turbulent Rayleigh–Bénard convection of fluids with temperature-dependent properties. *J. Fluid Mech.* **851**, 374–390.

XIA, K.-Q. 2013 Current trends and future directions in turbulent thermal convection. *Theor. Appl. Mech. Lett.* **3** (5), 052001.

YIK, H., VALORI, V. & WEISS, S. 2020 Turbulent Rayleigh–Bénard convection under strong non-Oberbeck–Boussinesq conditions. *Phys. Rev. Fluids* **5**, 103502.